Quantum Quenches in Chern Insulators

M. D. Caio,[1] N. R. Cooper,[2] and M. J. Bhaseen[1]
[1]Department of Physics, King's College London, Strand, London WC2R 2LS, United Kingdom
[2]T.C.M. Group, Cavendish Laboratory, J.J. Thomson Avenue, Cambridge CB3 0HE, United Kingdom
(Received 8 April 2015; published 2 December 2015)

We explore the nonequilibrium response of Chern insulators. Focusing on the Haldane model, we study the dynamics induced by quantum quenches between topological and nontopological phases. A notable feature is that the Chern number, calculated for an infinite system, is unchanged under the dynamics following such a quench. However, in finite geometries, the initial and final Hamiltonians are distinguished by the presence or absence of edge modes. We study the edge excitations and describe their impact on the experimentally observable edge currents and magnetization. We show that, following a quantum quench, the edge currents relax towards new equilibrium values, and that there is light-cone spreading of the currents into the interior of the sample.

DOI: 10.1103/PhysRevLett.115.236403 PACS numbers: 71.10.Pm, 03.65.Vf, 67.85.-d, 73.43.-f

Topological phases of matter display many striking features, ranging from the precise quantization of macroscopic properties, to the emergence of fractional excitations and gapless edge states. An important class of topological systems is provided by the so-called Chern insulators realized in two-dimensional settings [1]. A famous example is the Haldane model [2], which describes spinless fermions hopping on a honeycomb lattice. The Haldane model exhibits both topological and nontopological phases, and its behavior is closely related to the integer quantum Hall effect. Recent advances using ultracold atoms [3–7] have led to the experimental realization of the Haldane model [8]. Proposals also exist for realizing other states of topological matter using cold atoms [9].

A fundamental characteristic of topological systems is their robustness to local perturbations, making them ideal candidates for applications in metrology and quantum computation. However, much less is known about their dynamical response to global perturbations and time-dependent driving. This issue is of relevance in a variety of contexts, ranging from the time evolution and controlled manipulation of prepared topological states, to the dynamics of topological systems coupled to their environment. Understanding the impact of topology on the out of equilibrium response is crucial for further developments, and is the motivation for this present work. For recent progress in this direction see Refs. [10–18].

In this Letter we investigate the nonequilibrium dynamics of the paradigmatic Haldane model. In particular, we consider quantum quenches and sweeps between topological and nontopological phases. Key questions that we will address include the following. What happens to the topological properties on transiting between different phases? What happens to the edge excitations following a quantum quench? How do the topological characteristics influence the nonequilibrium dynamics?

Model.—The Haldane model describes spinless fermions hopping on a honeycomb lattice with both nearest and next nearest neighbor hopping parameters. The Hamiltonian is given by [2]

$$\hat{H} = t_1 \sum_{\langle i,j\rangle} (\hat{c}_i^\dagger \hat{c}_j + \text{H.c.}) + t_2 \sum_{\langle\langle i,j\rangle\rangle} (e^{i\varphi_{ij}} \hat{c}_i^\dagger \hat{c}_j + \text{H.c.}) + M \sum_{i\in A} \hat{n}_i - M \sum_{i\in B} \hat{n}_i, \quad (1)$$

where the fermionic operators obey the anticommutation relations $\{\hat{c}_j, \hat{c}_j^\dagger\} = \delta_{ij}$ and $\hat{n}_i \equiv \hat{c}_i^\dagger \hat{c}_i$. Here, $\langle i,j\rangle$ and $\langle\langle i,j\rangle\rangle$ indicate the summation over the nearest and next to nearest neighbor sites, respectively, and A and B label the two sublattices. The phase factor $\varphi_{ij} = \pm\varphi$ is introduced in order to break time-reversal symmetry and is positive for anticlockwise next to nearest neighbor hopping. The energy offset $\pm M$ breaks spatial inversion symmetry. The phase diagram of the Haldane model is shown in Fig. 1(a); following Ref. [2] we assume that $|t_2/t_1| \leq 1/3$ so that the bands may touch, but not overlap.

For $t_2, M \ll t_1$, the Hamiltonian (1) has a linear dispersion near the six corners of the hexagonal Brillouin zone, but only two of these are inequivalent. As a result, close to half filling, the low-energy description is given by the sum of two Dirac Hamiltonians

$$\hat{H}_\alpha = \begin{pmatrix} m_\alpha c^2 & -cke^{i\alpha\theta} \\ -cke^{-i\alpha\theta} & -m_\alpha c^2 \end{pmatrix}, \quad (2)$$

where $\alpha = \pm 1$ label the Dirac points. Here, $c = 3t_1/2\hbar$ is the effective speed of light, $k\exp(i\theta)$ parametrizes the 2D momentum (k_x, k_y), and $m_\alpha = (M - 3\sqrt{3}\alpha t_2 \sin\varphi)/c^2$ is the effective mass [2]. The topological phases have a nonvanishing Chern number ν [1,2,19,20]. For a state

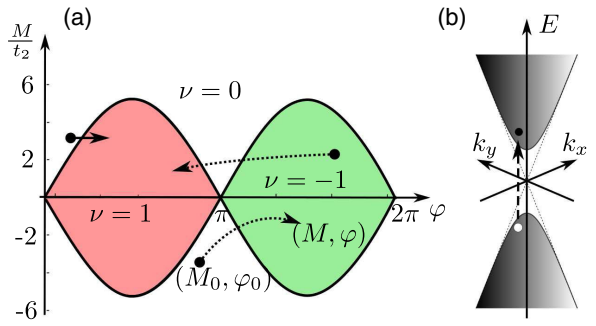

FIG. 1 (color online). (a) Phase diagram of the Haldane model obtained from the low-energy Dirac fermion representation, showing topological ($\nu = \pm 1$) and nontopological phases ($\nu = 0$) [2]. We consider quantum quenches and sweeps between different regions of the phase diagram, as illustrated by the arrows. (b) The low-energy spectrum of the Haldane model is described by excitations around two Dirac points. After a quench, carriers in the lower band are excited to the upper band.

$|\psi\rangle$ this is defined by the integral of the Berry curvature over the 2D Brillouin zone. In the low-energy description this corresponds to integration over 2D momentum space:

$$\nu = \frac{1}{2\pi}\int d^2k\ \Omega, \tag{3}$$

where $\Omega = \partial_{k_x} A_{k_y} - \partial_{k_y} A_{k_x}$ and $A_{k_\mu} = i\langle\psi|\partial_{k_\mu}|\psi\rangle$ is the Berry connection. For the ground state of the Haldane model $\nu \in \pm 1, 0$. This may be decomposed into contributions from the two Dirac points as $\nu = \nu_+ + \nu_-$, where $\nu_\alpha = -(\alpha/2)\mathrm{sgn}(m_\alpha) \in \pm 1/2$. The boundaries of the topological phases correspond to the locations where $m_\pm$ changes sign. They are thus given by $M/t_2 = \pm 3\sqrt{3}\sin\varphi$, and are independent of t_1, see Fig. 1.

Quantum quenches.—In order to gain insight into the nonequilibrium dynamics of the Haldane model, we consider quantum quenches between different points (M, φ) on the phase diagram shown in Fig. 1, for fixed values of t_1 and t_2. At time $t = 0$, we prepare our system in the ground state with parameters (M_0, φ_0). At half filling our initial state fills the lower band. We then abruptly change the parameters of $\hat{H}$ to (M, φ), and allow the system to evolve unitarily under the action of this new Hamiltonian. In general, this will lead to a nontrivial occupation of both the lower and the upper bands.

We begin by examining the nonequilibrium response of the effective Dirac Hamiltonian $\hat{H} = \hat{H}_+ + \hat{H}_-$. Since $\nu = -\frac{1}{2}[\mathrm{sgn}(m_+) - \mathrm{sgn}(m_-)]$, quenching between different phases corresponds to changing the sign of one or both of the masses m_α. For a given Dirac point, such changes will lead to a redistribution of carriers between the two bands, which may be measured through band-mapping techniques [8]. For a θ independent superposition, $|\psi_\alpha(k)\rangle = a_\alpha(k)e^{-iE^l_\alpha(k)t}|l_\alpha(k)\rangle + b_\alpha(k)e^{-iE^u_\alpha(k)t}|u_\alpha(k)\rangle$, the Chern number is formally given by

$$\nu_\alpha(t) = -\alpha \times \mathrm{sgn}(m_\alpha)\left(\frac{1}{2} - |b_\alpha(0)|^2\right) - |b_\alpha(\infty)||a_\alpha(\infty)|\cos[(E^u_\alpha(\infty) - E^l_\alpha(\infty))t + \delta], \tag{4}$$

where we integrate over the whole 2D momentum space. Here, $a_\alpha(k)$ and $b_\alpha(k)$ are complex c numbers, $\delta = \arg[a_\alpha(\infty)] - \arg[b_\alpha(\infty)]$, and $E^{l,u}_\alpha(k)$ are the energies in the lower and upper bands. In general, $\nu_\alpha(t)$ is time dependent, and differs from its ground state values $\pm 1/2$. However, the time dependence only enters via the superposition coefficients evaluated at $k = \infty$. An explicit computation shows that $b_\alpha(\infty) = 0$, following a quantum quench, see Fig. 2 and the Supplemental Material [21]. In addition, $b_\alpha(0) = 0, \pm 1$, so the potential modification of ν_α is compensated for by the change in sign of m_α. As a result the Chern number is unchanged from its initial value, even if one quenches between different phases. Similar results may also be obtained for a linear sweep, $m_\alpha(t) = t/\tau$, see the Supplemental Material [21].

Preservation of Chern number.—An intuitive way to understand the persistence of ν following a quantum quench is in terms of spin textures in momentum space. The Dirac Hamiltonian in Eq. (2) can be recast as an effective spin in a $\mathbf{k}$-dependent magnetic field $\mathbf{h}_\alpha(\mathbf{k})$. Explicitly, $\hat{H}_\alpha(\mathbf{k}) \equiv -\mathbf{h}_\alpha(\mathbf{k}) \cdot \boldsymbol{\sigma}/2$, where $\boldsymbol{\sigma}$ are the Pauli matrices. In equilibrium, the topological phases with $\nu_\alpha = \pm 1/2$ correspond to meron spin configurations, which wind on the upper (lower) half sphere [22]. Following a quantum quench, the spins precess in the effective magnetic field of the new Hamiltonian, preserving the topological characteristics of the initial spin configuration. A similar argument may also be applied to the Haldane model (1) in $\mathbf{k}$ space. Indeed, one expects the preservation of topological invariants under time evolution to

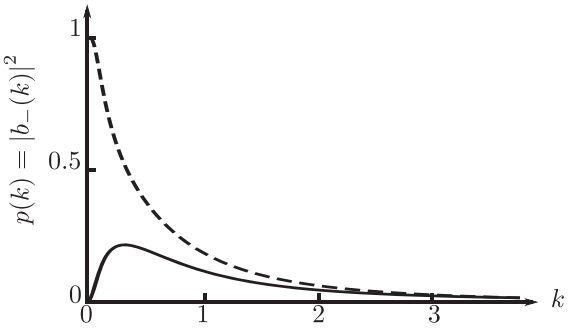

FIG. 2. Probability of occupying the upper band for a single Dirac point ($\alpha = -1$) with $c = 1$, following a quench of m_α. Sign-preserving quench, $m_- = -1 \to m'_- = -0.1$ (solid line), and a sign-changing quench, $m_- = -1 \to m'_- = 0.1$ (dashed line). In both cases, $b_-(\infty) = 0$, corresponding to the time independence of $\nu_-(t)$ using Eq. (4). The sign-changing quench yields $|b_-(0)|^2 = 1$, but the contribution to $\nu_-(t)$ in Eq. (4) is compensated by the change in sign of m_-. As a result, ν_- is unchanged from its initial value.

be a general feature for noninteracting fermions in a periodic system, where each $\mathbf{k}$ state evolves unitarily under some Hamiltonian $\hat{H}(\mathbf{k})$, provided $\hat{H}(\mathbf{k})$ is smoothly varying in $\mathbf{k}$ space. The persistence of the topological invariant of a state, even under changes in the topology of the underlying Hamiltonian, has also been noted in the context of quenches of topological superfluid states [23,24]. In principle, the preservation of the Chern index may be measured experimentally by expansion-imaging techniques, which can allow the wave functions of the occupied single particle states to be fully determined across the Brillouin zone [4,17,25,26]. It is important to stress, however, that this does not imply the preservation of the Hall response. The latter depends on the final state Hamiltonian, not just the initial state. Out of equilibrium, the usual Thouless-Kohmoto-Nightingale-den Nijs (TKNN) formula [1] does not apply [27].

Edge states.—In the above discussion we have demonstrated that the value of ν is unchanged as one quenches and sweeps between different phases. However, there is a fundamental distinction between the topological and nontopological phases, due to the presence or absence of edge states in a finite-size sample [28]. In quenching between phases of different topological character, these edge states will either appear or disappear, depending on the direction of the quench. This is confirmed in Fig. 3, which shows the reconstruction and repopulation of the energy levels following a quench from the nontopological phase to a topological phase. It is readily seen that the edge states emerge and are populated as a result of the quench, in spite of the fact that ν remains equal to zero in the absence of boundaries. Conversely, a quench from a topological phase to the nontopological phase eliminates the edge states, while ν remains pinned at unity.

Edge currents and orbital magnetization.—Having examined the repopulation of the edge states we now consider physical observables that depend on these states, including the edge currents and the orbital magnetization. We first consider these quantities in equilibrium, which already display interesting features. We define the local current flowing through the site i by $\hat{\mathbf{J}}_i = -\frac{i}{2}\sum_j \boldsymbol{\delta}_{ji}(t_{ij}\hat{c}_i^\dagger \hat{c}_j - \text{H.c.})$, where t_{ij} is the hopping parameter of the Haldane model between sites i and j, $\boldsymbol{\delta}_{ji}$ is the vector displacement of site i from j, and the sum is over the nearest and next nearest neighbors. The site indices may be decomposed into the triplet $\{m, n, s\}$ labeling the x and y positions of the unit cell and the sublattice index $s = A, B$. The total longitudinal current flowing along the strip in the x direction at a definite transverse y position is therefore given by $J_n^x = \langle \hat{J}_n^x \rangle = \sum_{ms} \langle \hat{J}_{mns}^x \rangle$. In Fig. 4(a) we plot this current within the topological phase for $M = 0$ and $\varphi = \pi/3$. The presence of the counterpropagating edge currents is readily seen. In Fig. 4(b) we show the dependence of these edge currents on φ where, for clarity, we define the edge currents precisely on the sample boundaries. Measurements of edge currents have been performed for ladder systems [29], and other forms of local imaging have been proposed [30]. Somewhat surprisingly, the edge currents vanish on loci within the topological phase, in spite of the presence of edge states in the spectrum. The edge currents are composed of counterpropagating contributions, which cancel at $\varphi = \pi/2$, see the Supplemental Material [21]. Moreover, the longitudinal currents J_n^x exhibit π periodicity in φ. This is a consequence of being at half filling and occurs in spite of the fact that the Hamiltonian and the current operator have a periodicity of 2π. To prove the π periodicity in φ we first note that both the Hamiltonian and the current operator change sign under the transformation $M \to -M$, $\varphi \to \varphi + \pi$, $\hat{c}_{mnA} \to \hat{c}_{mnA}$, $\hat{c}_{mnB} \to -\hat{c}_{mnB}$, thereby interchanging the upper and the lower bands. At half filling, we fill only the lower band, and it follows that $J_n^x(M, \varphi) = J_n^x(-M, \varphi + \pi)$. In addition, the current changes sign under the parity transformation $x \to -x$. This interchanges the sublattices and corresponds to $M \to -M$ and $\varphi \to -\varphi$. It follows that $J_n^x(M, \varphi) = -J_n^x(-M, -\varphi) = J_n^x(-M, \varphi)$, where in the last step we use the transformation properties under time reversal. Combining these relations, one obtains the π periodicity in φ and the vanishing of the longitudinal currents for $\varphi = \pi/2$.

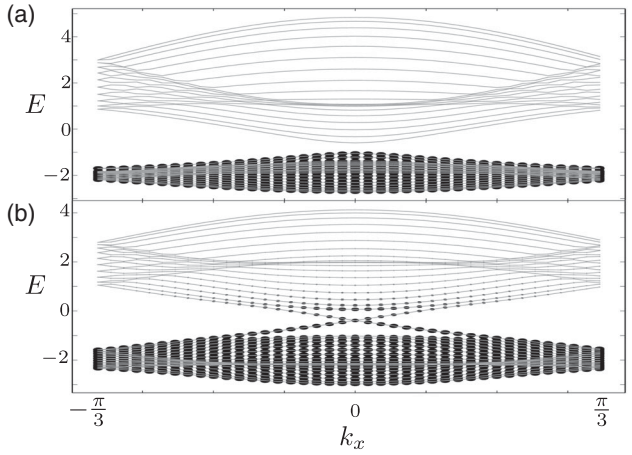

FIG. 3. Energy spectrum of the Haldane model obtained by exact diagonalization on a finite-size strip of width $N = 20$ unit cells with armchair edges. We take periodic (open) boundary conditions along (transverse to) the strip and set $t_1 = 1$, $t_2 = \frac{1}{3}$, and $M = 1$. (a) Equilibrium population of the energy levels in the nontopological phase with $\varphi = \pi/6$. (b) Repopulation of the levels after a quench to the topological phase with $\varphi = \pi/3$, corresponding to the solid arrow in Fig. 1(a). The size of the dots is proportional to the probability of finding a particle in the mode. Postquench, the filling of the edge states and the bands is nontrivial.

Similar arguments also apply to the (lattice discretization of the) orbital magnetization:

$$\mathcal{M} = \frac{1}{2\mathcal{A}} \int d^2 r \, \mathbf{r} \times \langle \hat{\mathbf{J}}(\mathbf{r}) \rangle, \tag{5}$$

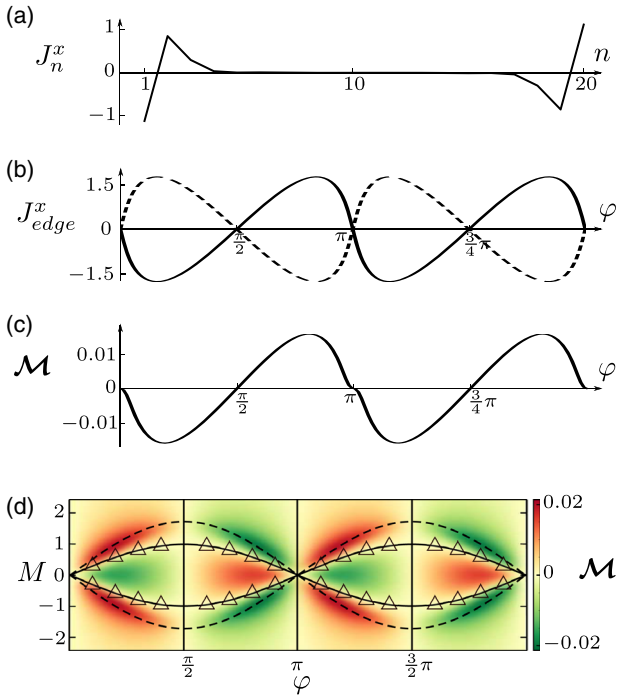

FIG. 4 (color online). Equilibrium properties of the Haldane model on a finite-size strip as used in Fig. 3. (a) Total longitudinal current J^x_n along the strip as a function of the transverse spatial index $n \in 1, \ldots, 20$, for $M = 0$ and $\varphi = \pi/3$. (b) Edge currents corresponding to J^x_n with $n = 1$ (solid) and $n = 20$ (dashed) for $M = 0$. The edge currents exhibit π periodicity in φ and vanish when $\varphi = \pi/2$. (c) Orbital magnetization $\mathcal{M}$ as a function of φ for $M = 0$. (d) Intensity plot of $\mathcal{M}$ where the dashed lines correspond to the boundaries of the topological phases. Numerically, we observe that $\mathcal{M}$ vanishes on the loci $M = \pm \sin\varphi$ (solid) within the topological phases. The loci are fits to the numerical data (triangles) where $\mathcal{M} = 0$. The magnetization also vanishes on the vertical lines $\varphi = \pi/2, \pi, 3\pi/2, \ldots$, as follows from symmetry considerations.

where $\hat{\mathbf{J}}(\mathbf{r})$ is the local current density operator and $\mathcal{A}$ is the area. As shown in Fig. 4(c) this also vanishes within the topological phases and has π periodicity in φ [31,32]. Our numerical computations also reveal that the magnetization vanishes on a sinusoidal locus $M = \pm \sin(\varphi)$ within the topological phases, see Fig. 4(d). In addition, $\mathcal{M}(M, \varphi)$ has extrema at $M = 0$ and on the topological phase boundaries, $M = \pm\sqrt{3}\sin(\varphi)$, for fixed φ. Away from half filling, the particle-hole symmetry is broken and the periodicity of the currents and the magnetization is restored to 2π. The increase or decrease of the edge currents depends on the sign of the doping and the Chern index, see the Supplemental Material [21].

Dynamics of the edge currents.—Having discussed the equilibrium properties of the edge currents we now consider their response to quantum quenches. In Fig. 5 we show quenches from the topological to the nontopological phase. The edge currents decay towards new values that are numerically close, but not equal, to the equilibrium values

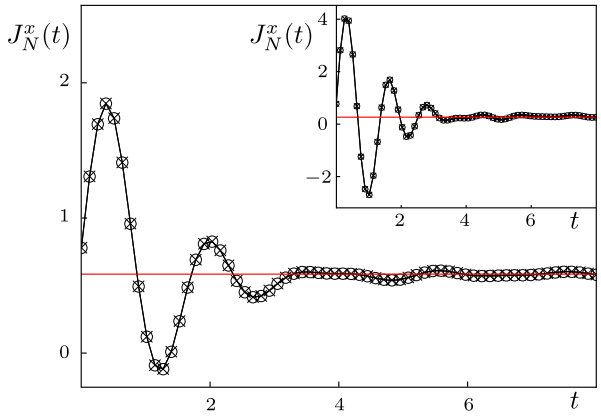

FIG. 5 (color online). Dynamics of the edge current $J^x_N(t)$ for $N = 30$ (circles) and $N = 40$ (crosses) following a quantum quench between the topological phase and the nontopological phase with $t_1 = 1$, $t_2 = \frac{1}{3}$, and fixed $\varphi = \pi/3$. Quenches from $M = 1.4$ to $M = 1.6$ (main panel) and from $M = 1.4$ to $M = 2.2$ (inset) showing that the edge currents approach new equilibrium values. For the chosen parameters, these are very close to the ground state expectation values of J^x_N in the final Hamiltonian, as indicated by the horizontal lines.

of the postquench Hamiltonian. This is in spite of the fact that the system is left in an excited state under unitary evolution, and that ν remains pinned to unity in the absence of boundaries. Quenches from the nontopological to topological phases exhibit similar behavior, see the Supplemental Material [21]. Further insight into the nonequilibrium evolution may be gleaned from the time evolution of the longitudinal currents across the two-dimensional system. As shown in Fig. 6, the damped oscillations of the edge currents are accompanied by the light-cone spreading of the currents into the interior of the

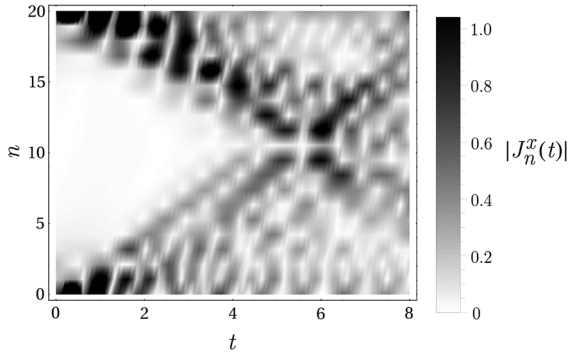

FIG. 6. Dynamics of the currents $|J^x_n(t)|$ following a quantum quench from the topological to the nontopological phase for the parameters used in the inset of Fig. 5. The damped oscillations of the edge currents are clearly visible, as is the light-cone spreading of the currents into the interior of the sample, where $c = 3t_1/2\hbar = 3/2$ is the effective speed of light. The waves propagating from the two edges meet at time $t \sim (N/2)\sqrt{3}/2c \sim 5.77$, leading to resurgent oscillations in finite-size samples, see the Supplemental Material [21].

sample. It would be interesting to observe this dynamics in experiment, which is in principle possible if local imaging is available [30].

Conclusions.—In this Letter we have explored the nonequilibrium dynamics of the Haldane model. We have demonstrated that the Chern number is preserved in both quenches and sweeps between different regions of the phase diagram. However, the edge states may be reconstructed and repopulated, leading to changes in the accompanying edge currents. Predictions for experiment include the vanishing of the equilibrium edge currents in the topological phases, and the light-cone spreading of the currents following a quantum quench. There is a wide variety of directions for further research, including the dynamics of the conductivity and its relation to the Chern number, and the role of decoherence via coupling to the environment.

This work was supported by EPSRC Grants No. EP/J017639/1 and No. EP/K030094/1. M. J. B. thanks the EPSRC Centre for Cross-Disciplinary Approaches to Non-Equilibrium Systems (CANES) funded under Grant No. EP/L015854/1. M. J. B. and M. D. C. thank the Thomas Young Center for support.

Note added.—The related paper [33] also reached similar conclusions to ours regarding the invariance of ν under unitary evolution.

[1] D. J. Thouless, M. Kohmoto, M. P. Nightingale, and M. den Nijs, Phys. Rev. Lett. **49**, 405 (1982).
[2] F. D. M. Haldane, Phys. Rev. Lett. **61**, 2015 (1988).
[3] N. Goldman, A. Kubasiak, A. Bermudez, P. Gaspard, M. Lewenstein, and M. A. Martin-Delgado, Phys. Rev. Lett. **103**, 035301 (2009).
[4] E. Alba, X. Fernandez-Gonzalvo, J. Mur-Petit, J. K. Pachos, and J. J. Garcia-Ripoll, Phys. Rev. Lett. **107**, 235301 (2011).
[5] M. Aidelsburger, M. Atala, S. Nascimbène, S. Trotzky, Y.-A. Chen, and I. Bloch, Appl. Phys. B **113**, 1 (2013).
[6] N. Goldman, E. Anisimovas, F. Gerbier, P. Öhberg, I. B. Spielman, and G. Juzeli Åńnas, New J. Phys. **15**, 013025 (2013).
[7] A. R. Wright, Sci. Rep. **3**, 2736 (2013).
[8] G. Jotzu, M. Messer, R. Desbuquois, M. Lebrat, T. Uehlinger, D. Greif, and T. Esslinger, Nature (London) **515**, 237 (2014).
[9] F. Setiawan, K. Sengupta, I. B. Spielman, and J. D. Sau, arXiv:1503.07167.
[10] B. Dóra and R. Moessner, Phys. Rev. B **83**, 073403 (2011).
[11] T. Uehlinger, D. Greif, G. Jotzu, L. Tarruell, T. Esslinger, L. Wang, and M. Troyer, Eur. Phys. J. Spec. Top. **217**, 121 (2013).
[12] E. Perfetto, Phys. Rev. Lett. **110**, 087001 (2013).
[13] R. Barnett, Phys. Rev. A **88**, 063631 (2013).
[14] A. A. Patel, S. Sharma, and A. Dutta, Eur. Phys. J. B **86**, 367 (2013).
[15] G. Kells, D. Sen, J. K. Slingerland, and S. Vishveshwara, Phys. Rev. B **89**, 235130 (2014).
[16] A. Dutta, R. R. P. Singh, and U. Divakaran, Europhys. Lett. **89**, 67001 (2010).
[17] P. Hauke, M. Lewenstein, and A. Eckardt, Phys. Rev. Lett. **113**, 045303 (2014).
[18] L. Stojchevska, I. Vaskivskyi, T. Mertelj, P. Kusar, D. Svetin, S. Brazovskii, and D. Mihailovic, Science **344**, 177 (2014).
[19] S.-S. Chern, Ann. Math. **47**, 85 (1946).
[20] M. V. Berry, Proc. R. Soc. A **392**, 45 (1984).
[21] See Supplemental Material at http://link.aps.org/supplemental/10.1103/PhysRevLett.115.236403 for further details.
[22] E. Fradkin, *Field Theories of Condensed Matter Physics*, 2nd ed. (Cambridge University Press, Cambridge, England, 2013).
[23] M. S. Foster, M. Dzero, V. Gurarie, and E. A. Yuzbashyan, Phys. Rev. B **88**, 104511 (2013).
[24] M. S. Foster, V. Gurarie, M. Dzero, and E. A. Yuzbashyan, Phys. Rev. Lett. **113**, 076403 (2014).
[25] E. Zhao, N. Bray-Ali, C. J. Williams, I. B. Spielman, and I. I. Satija, Phys. Rev. A **84**, 063629 (2011).
[26] N. Fläschner, B. S. Rem, M. Tarnowski, D. Vogel, D. S. Lühmann, K. Sengstock, and C. Weitenberg, arXiv:1509.05763.
[27] M. D. Caio, N. R. Cooper, and M. J. Bhaseen (to be published).
[28] N. Hao, P. Zhang, Z. Wang, W. Zhang, and Y. Wang, Phys. Rev. B **78**, 075438 (2008).
[29] M. Atala, M. Aidelsburger, M. Lohse, J. T. Barreiro, B. Paredes, and I. Bloch, Nat. Phys. **10**, 588 (2014).
[30] N. Goldman, J. Dalibard, A. Dauphin, F. Gerbier, M. Lewenstein, P. Zoller, and I. B. Spielman, Proc. Natl. Acad. Sci. U.S.A. **110**, 6736 (2013).
[31] T. Thonhauser, D. Ceresoli, D. Vanderbilt, and R. Resta, Phys. Rev. Lett. **95**, 137205 (2005).
[32] D. Ceresoli, T. Thonhauser, D. Vanderbilt, and R. Resta, Phys. Rev. B **74**, 024408 (2006).
[33] L. D'Alessio and M. Rigol, Nat. Commun. **6**, 8336 (2015).